Heat Transfer to Fine Powders in a Bubbling Fluidized Bed with Sound Assistance

DeShau Huang and Edward Levy
Energy Research Center, Lehigh University, Bethlehem, PA 18015

Most of the published research on heat transfer in a fluidized bed is focused on Geldart type B and D particles, while there is little information available on heat transfer to fine powders (Geldart group C). Previous studies of fine powder fluidization with sound assistance have shown that stable bubbling can be achieved with sound assistance. In this study, experiments were performed to measure bubble behavior and heat-transfer coefficients around a horizontal tube in a fine powder fluidized bed with sound assistance. Two types of data are presented as functions of excess air velocity and sound pressure level—average and local heat-transfer coefficients and bubble frequency, packet residence time, and the fraction of the particle packet contact time. A packet renewal model with a gas film at the tube surface is proposed to explain the heat-transfer data. © 2004 American Institute of Chemical Engineers *AIChE J,* 50: 302–310, 2004
Keywords: fluidization, heat transfer, bubbling, fine powders

Introduction

Geldart Group C particles are difficult to fluidize with conventional techniques due to strong cohesive forces between particles. Past research on cohesive powders has shown that vibrations can disrupt interparticle forces and thereby improve fluidization (Morse, 1955). In the presence of acoustic vibration, particle clusters break up into subclusters, thus preventing spouting and channeling in the bed (Chirone and Massimilla, 1994; Russo et al., 1995), and promoting more uniform fluidization, bed expansion, and bubbling (Herrera, 2000). Previous research has also shown that high intensity sound reduces the minimum bubbling velocity.

Studies of heat transfer in a fluidized bed with a horizontal tube have been carried out by many investigators, with the most complete understanding of the heat-transfer process obtained for Geldart B and D powders (Vreedenberg, 1958; Adams and Welty, 1979; Decker and Glicksman, 1983). There is very little information available on heat transfer in Type A and C powders.

The studies with B and D particles have demonstrated that heat-transfer coefficients are related to the volumetric heat capacity of the particles, the particle diameter, the thermal conductivity of fluidizing gas (Grewal and Saxena, 1980), and bubbling characteristics in the bed (Chen and Tuzla, 1996).

Miyamoto et al. (1997) found that heat transfer is enhanced by the particle movement. In addition, Ozkaynak and Chen (1980) found that a higher bubble frequency caused a shorter packet residence time, and this led to good heat transfer. In large particle fluidized beds, Moslemian et al. (1991) concluded that the manner in which the superficial gas velocity influenced the local and average heat transfer from a horizontal tubular surface depended strongly on the location of the surface in the bubbling bed. The overall heat-transfer coefficient on a single tube at first increased with an increase in fluidization velocity, reached a maximum, and then decreased slightly or tended to be constant with further increasing velocity. Olsson and Almstedt (1995) investigated the influence of excess gas velocity on the local instantaneous and time-averaged heat transfer in a fluidized bed. The bubbles caused a rapid mixing in the bed, which led to high heat-transfer rates between the bed and immersed surface, and between the gas and particles. They demonstrated that the high correlation between the heat-transfer coefficient and the local bubble frequency reflected, to a large extent, the coupling between the frequency with which the particles near the tube surface were being re-

Correspondence concerning this article should be addressed to E. K. Levy at eklo@lehigh.edu.

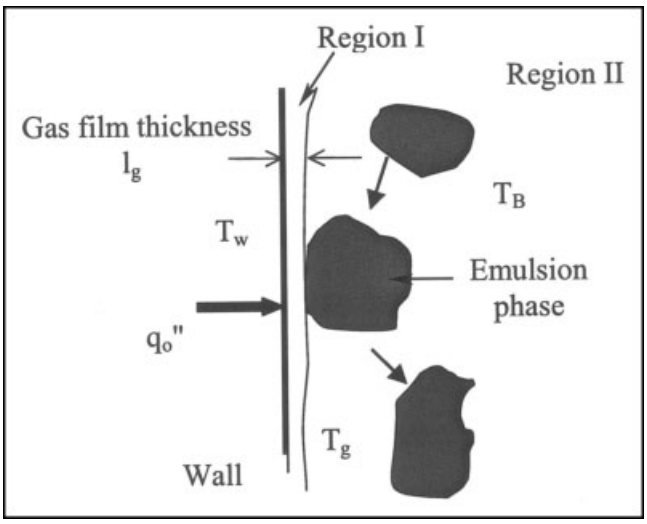

Figure 1. Heat-transfer mechanism for packet renewal model with a gas film.

placed by fresh, thermally unaffected particles. In a like manner, Wiman and Almstedt (1997) indicated that the heat-transfer coefficient was strongly coupled with the bubble frequency.

This article describes the heat transfer from a horizontal tube and bubble behavior in a fine powder fluidized bed with sound assistance. Experiments were performed to obtain local and average heat-transfer coefficients, gas film thickness, and data on bubble frequency and packet residence time at the tube surface. These data, obtained as functions of sound pressure level and excess gas velocity, were used to relate heat-transfer coefficient to bed bubbling conditions. A packet renewal model with a gas film at the tube surface is proposed to explain the heat-transfer data.

Theoretical Model Development

The overall heat-transfer coefficient between a tube surface and the bed is composed of three components: bubble phase convection, dense (emulsion) phase convection, and radiation. Radiation heat transfer is usually not significant if the bed temperature is far below 700°C. According to previous studies

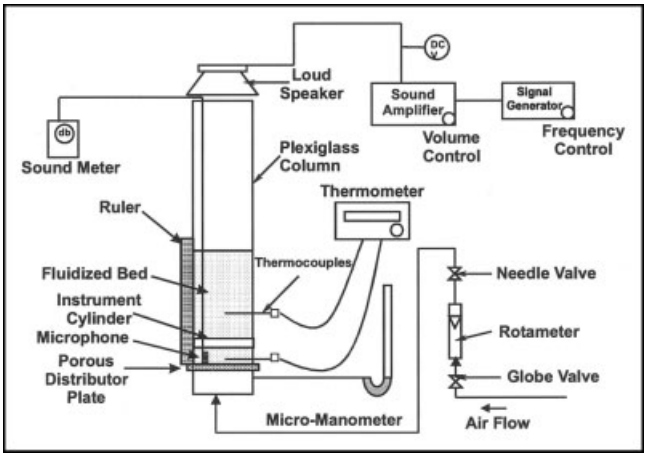

Figure 2. Fluidized-bed apparatus.

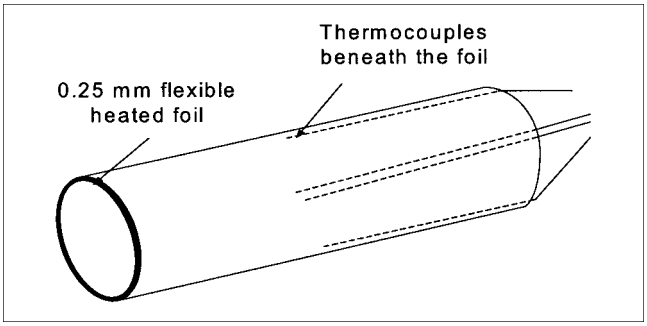

Figure 3. Configuration of the heated tube.

(Botterill, 1975), the convective heat transfer from the bubble phase is much less than that of the emulsion phase, and, thus, the overall heat transfer is dominated by the emulsion phase in a bubbling bed. Therefore, neglecting bubble phase heat transfer and radiation, the heat-transfer coefficient is expressed as

$$h = (1 - F_b) \cdot h_d = F_d \cdot h_d \tag{1}$$

The classical packet renewal model proposed by Mickley and Fairbanks (1955) is concerned with heat transfer from the heated surface to packets of particles. From the present experimental results for fine powders, there exists a gas film in the vicinity of the heated surface. The classical packet renewal model for heat transfer in a fluidized bed has been modified to account for a gas film thickness at the heated surface.

The heat-transfer mechanism at the heated surface is shown in Figure 1. Region I is the gas film between the wall and the emulsion phase and bubbles. Region II represents the emulsion phase and bubble phase, which alternatively come into contact with the gas film.

In Region II, heat transfer takes place by unsteady-state conduction from the gas film into the emulsion phase. The governing equation is the one-dimensional (1-D) transient heat conduction equation.

$$\frac{\partial^2 T}{\partial x^2} = \frac{1}{\alpha_d} \frac{\partial T}{\partial t} \tag{2}$$

with the boundary conditions for constant heat flux

$$T(x, 0) = T_B \qquad -k_d \frac{\partial T}{\partial x} = q_o'' @\ x = 0 \qquad T(\infty, t) = T_B \tag{3}$$

Using the similarity variable approach, $\eta = x/\sqrt{4\alpha_d t}$, an analytical solution can be obtained (Incropera and Dewitt, 1999)

$$T(x, t) - T_B = \frac{2q_o''(\alpha_d t/\pi)^{1/2}}{k_d} \exp\left(\frac{-x}{4\alpha_d t}\right) - \frac{q_o'' x}{k_d} \operatorname{erfc}\left(\frac{x}{2\sqrt{\alpha_d t}}\right) \tag{4}$$

where erfc is the complementary error function. At $x = 0$, the interface temperature is

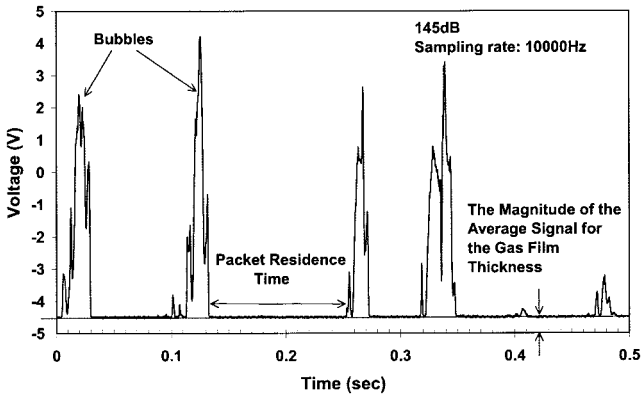

Figure 4. Voltage signal output.

$$T(0, t) - T_B = \frac{2q''_o(\alpha_d t/\pi)^{1/2}}{k_d} \tag{5}$$

In Region I, there is a gas film of thickness l_g existing between the heated surface and the emulsion phase and bubbles. Neglecting transient effects within the gas film, steady-state conduction heat transfer occurs in Region I. Therefore

$$\Delta T_g = \frac{q''_o \cdot l_g}{k_g} \tag{6}$$

The instantaneous heat-transfer coefficient is represented by

$$h_d(t) = \frac{q''_o}{T_W - T_B} \tag{7}$$

where the wall temperature T_w is

$$T_W = T(0, t) + \Delta T_g \tag{8}$$

Substituting Eqs. 5, 6, and 8 into Eq. 7, the instantaneous heat-transfer coefficient is expressed as

$$h_d(t) = \frac{A}{t^{1/2} + A\,\dfrac{l_g}{k_g}} \tag{9}$$

where $A = \frac{1}{2}\sqrt{\pi\rho_d c_d k_d}$

Therefore, the time-average heat-transfer coefficient is expressed as

$$\overline{h_d} = \frac{1}{t_p}\int_0^{t_p} h_d(\tau)d\tau = \frac{2A}{\sqrt{t_p}}\left[1 - \frac{A}{\sqrt{t_p}}\frac{l_g}{k_g}\ln\left(\frac{\sqrt{t_p} + A\,\dfrac{l_g}{k_g}}{A\,\dfrac{l_g}{k_g}}\right)\right] \tag{10}$$

The time-average heat-transfer coefficient h in a fluidized bed for constant heat flux is obtained in Eq. 11

$$h = (1 - F_b)\cdot\overline{h_d} = F_d\cdot\sqrt{\frac{\pi\rho_d c_d k_d}{t_p}} \times\left[1 - \frac{1}{2}\sqrt{\frac{\pi\rho_d c_d k_d}{t_p}}\cdot\frac{l_g}{k_g}\ln\left(\frac{\sqrt{t_p} + \dfrac{1}{2}\sqrt{\pi\rho_d c_d k_d}\cdot\dfrac{l_g}{k_g}}{\dfrac{1}{2}\sqrt{\pi\rho_d c_d k_d}\cdot\dfrac{l_g}{k_g}}\right)\right] \tag{11}$$

The parameters of density, heat capacity, and thermal conductivity in Eq. 11 are treated as the bulk properties of the emulsion phase (Ranz, 1954; Kunii and Smith, 1960; Ozkaynay and Chen, 1980).

In the heat-transfer Eq. 11, as the gas film thickness approaches zero, the heat-transfer coefficient becomes

$$h = F_d\sqrt{\frac{\pi\rho_d c_d k_d}{t_p}} \tag{12}$$

Thus, in the limiting case at zero gas film thickness, Eq. 12 is the same as the heat-transfer coefficient of the classical packet renewal model.

Experimental Method

Fluidized-bed equipment

The experimental equipment, illustrated in Figure 2, consisted of a fluidized bed, a sound wave generation system, and a horizontal cylinder. The fluidized bed, a 152 mm ID cylindrical Plexiglas column, was equipped with a porous plate. The air flow rate was controlled by a needle valve, and a rotameter was used to measure the air flow rate.

The acoustic generation system included a digital signal generator, a sound amplifier, and a loudspeaker. The sound amplifier was used to generate acoustic intensity, and the digital signal generator manipulated acoustic frequency. A loudspeaker positioned on the top of the bed column was used to generate the acoustic waves. The microphone, which was

Table 1. Properties of the Fluidized Materials and of Air at Standard Conditions.

Material	$\overline{d_p}$ (μm)	c_p (J/kg/K)	k_p (W/m/K)	ρ_p (kg/m^3)	Geldart Classification
Glass Beads	820	753.6	0.89	2100	B
Fly Ash HC	82.5	1320	3.1	1720	A
Fly Ash BW	8.1	992.1	3.1	2283	C
Fly Ash SH	19.5	1050	3.1	2150	A–C
Talc	15.3	1062.5	0.191	2755	C
Air	N/A	1,005	0.0263	1.205	N/A

connected to a sound meter, was placed at the bottom of the bed to measure sound pressure level.

The experiments described in this article were performed with bed depths of 10 to 12 cm, an acoustic frequency of 80 Hz, and sound pressure levels at the distributor (SPL_o) from 88 to 150 db. For the powders tested, this combination of frequency and bed depth gave the largest values of SPL_o, with the sound pressure level increasing from the free surface of the bed to the distributor. (See Herrera et al. (2002) for a discussion of acoustic standing waves in fluidized beds.)

Instrumentation

Two instrumented cylinders with diameters of 16 mm were separately installed horizontally through the center of the bed at 50 mm above the distributor. One was used to determine heat-transfer coefficient and the other provided data on bubble behavior.

The heated cylinder, shown in Figure 3, was covered by a 528-ohm flexible heating foil with 0.25 mm thickness. Four K-type wire thermocouples were placed at the surface at 90° intervals to measure the surface temperature. The foil was uniformly heated by an electrical current. Heat generation was obtained from Eq. 13

$$Q = \frac{V^2}{R} \tag{13}$$

The bed temperature was measured by four other K-type thermocouples placed at different elevations above the distributor. An average heat-transfer coefficient was calculated by Eq. 14

$$h = \frac{q''_o}{T_s - T_B} = \frac{V^2}{R \cdot A_s \cdot (T_s - T_B)} \tag{14}$$

where T_s is the average surface temperature and T_B is the average bed temperature.

An optical fiber probe was built into the other tube to detect bubble frequency and packet residence time at the tube surface. The tip of the probe was constructed from two optical fibers with diameters of 650 μm. The fibers were connected to a signal-processing unit. LED light was emitted along one fiber toward the particles, and the light reflected from the particles near the probe tip was received by the other fiber. When the signal-processing unit received a signal, it was transmitted to an analog to digital converter (ADC) with 12-bit resolution to analyze the signal. Its uncertainty is 2.4 μV.

A typical voltage vs. time signal is shown in Figure 4. Once a bubble passes by the probe tip, the receiving fiber will capture the reflected light intensity and have a voltage signal reaction, illustrated in Figure 4. In contrast, if particles are in contact with the probe tip, almost all the light will be blocked, and a very weak light intensity will be transmitted by the receiving fiber. Interpretation of this weak light intensity leads to a measurement of the packet residence time, such as shown in Figure 4. The amplitude of the voltage signal in the presence of a packet can be used to indicate the gas film thickness between the tip of the probe and the packet material.

Data are presented here from experiments performed on five types of particles, whose mean diameters and particle properties are listed in Table 1. The mean diameters of these particles were evaluated by Eq. 15

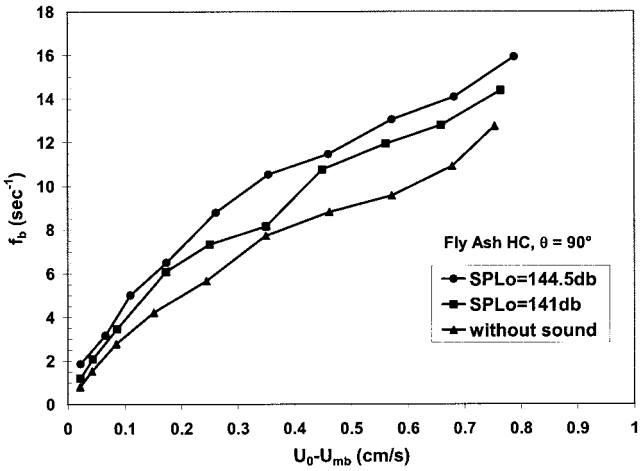

Figure 6. Variation of bubble frequency with excess air velocity.

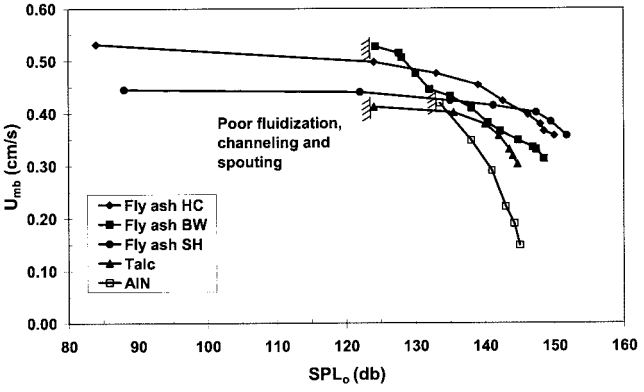

Figure 5. Variation of minimum bubbling velocity with SPL_o.

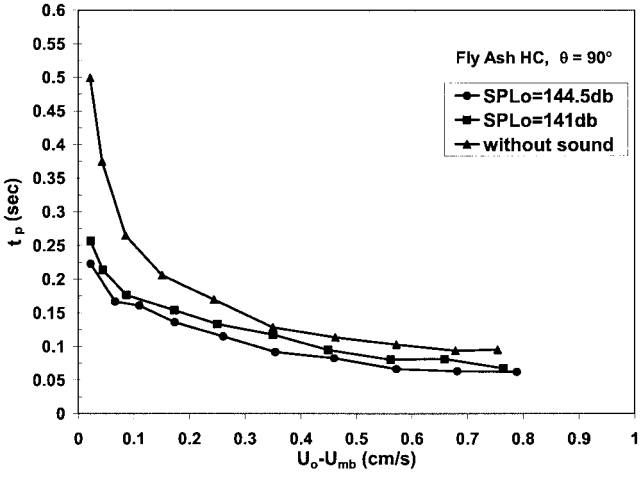

Figure 7. Variation of packet residence time with excess air velocity.

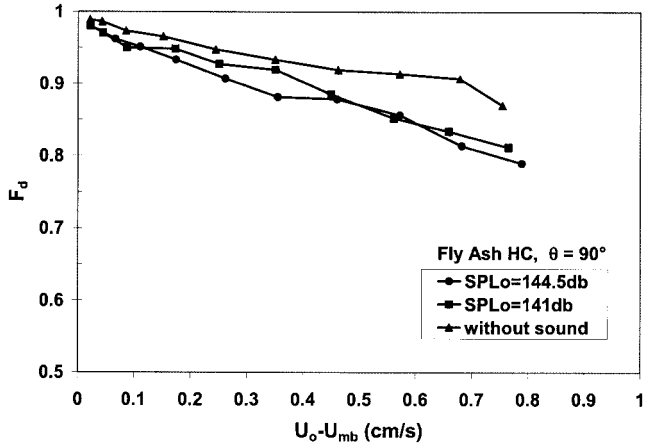

Figure 8. Fraction of packet contact time with excess air velocity.

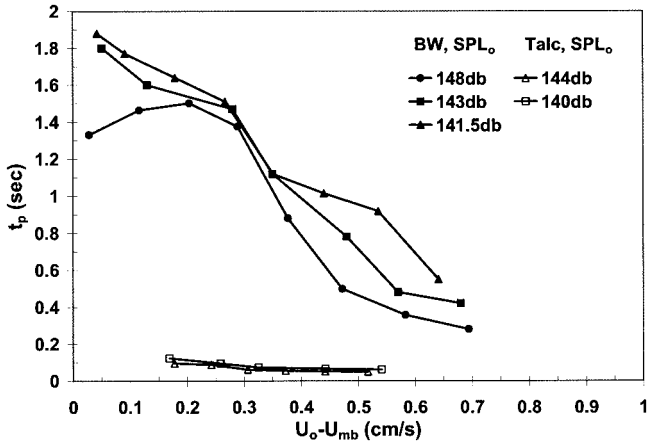

Figure 10. Variation of packet residence time with excess air velocity.

$$\overline{d_p} = \frac{1}{\sum x_i / d_i} \tag{15}$$

Results and Discussion

Bubble behavior

At a specific sound pressure level and acoustic frequency, the fluidization of fine powders progressed from a packed bed to an expanded bed, and then to bubbling with an increase of air velocity. After vigorous bubbling was obtained, the air velocity gradually was reduced. The minimum bubbling velocity was determined as bubbles began to disappear at the free surface.

Figure 5 shows the change in the minimum bubbling velocity with the SPL_o, defined as the sound pressure level (see Appendix A for the definition) at the distributor in a fluidized bed (Herrera, 2000). Without introducing acoustics, the background SPL_o was approximately 88 db. Fly ash HC and SH, which are Geldart type A powders, were easily fluidized without sound. The type C powders, Talc and fly ash BW, could not be fluidized without sound assistance. The data show that, once fluidized, minimum bubbling velocity decreased with an increase in SPL_o.

Figures 6–8 show the bubble behavior at the tube surface at $\theta = 90°$ measured from the bottom of the tube in a counterclockwise direction. Figure 6 shows the variation of bubble frequency with excess air velocity at different sound pressure levels for fly ash HC. The bubble frequency increased with an increase in excess air velocity. Figure 6 also shows that with sound assistance the bubble frequency was higher than without sound, and the bubble frequency increased with SPL_o for a fixed excess air velocity. Bubble formation is dependent on the physical structure of the particle clusters and on excess air velocity. According to previous studies of fine powder fluidization in an acoustic field (Chirone and Massimilla, 1994; Russo et al., 1995), a higher sound pressure level breaks up particle subclusters more easily. This, presumably, is the cause of the increase in bubble frequency with sound pressure level. To estimate the impact of sound on cluster size, calculations were performed for the fly ash BW data in Figure 5 using the Wen and Yu (1966) correlation for minimum fluidization velocity. These indicate a reduction in effective cluster diameter from 85 μm to 67 μm, as SPL_o was increased from 123 to 150 db.

Figure 7 shows the variation of packet residence time with excess air velocity for different sound pressure levels for fly

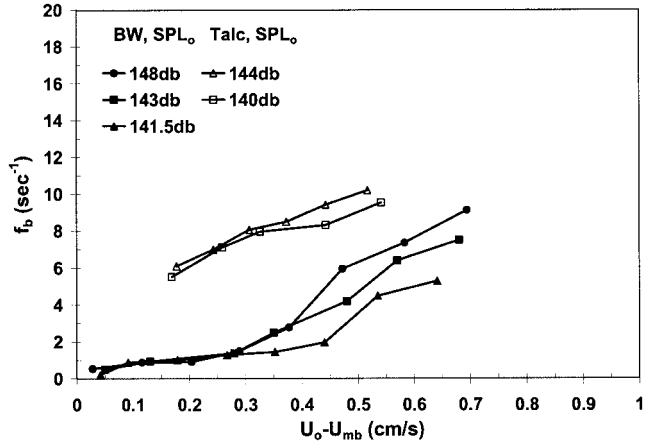

Figure 9. Variation of bubble frequency with excess air velocity.

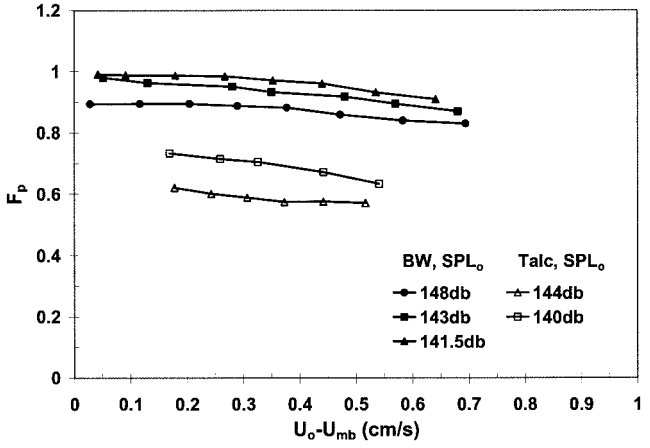

Figure 11. Variation of the fraction of packet contact time with excess air velocity.

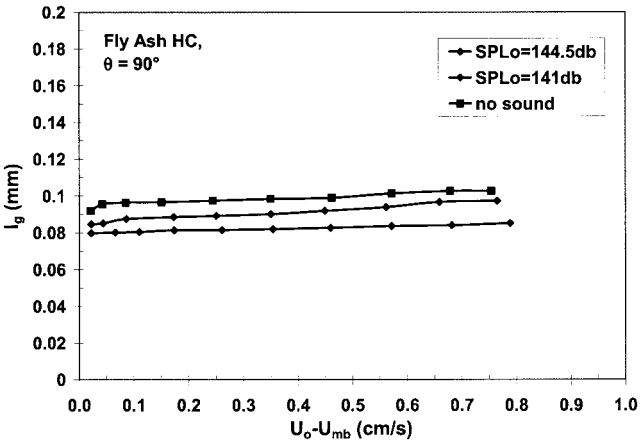

Figure 12. Variation of gas film thickness with excess air velocity for fly ash HC.

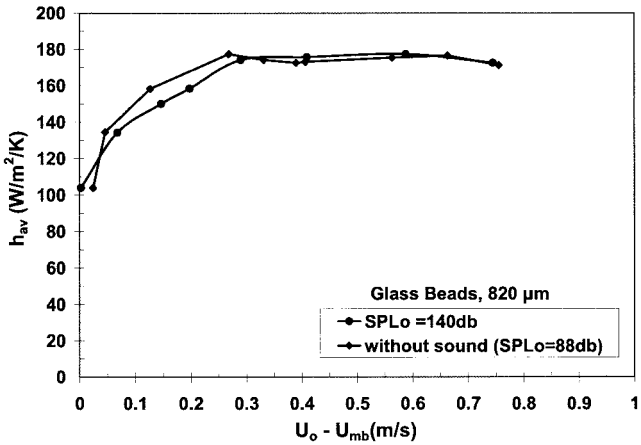

Figure 14. Comparison of sound effect on the average heat-transfer coefficients for glass beads.

ash HC. The packet residence time is related to bubble frequency; and, as the bubble frequency increased, the frequency of particle packet renewal at the tube surface also increased. As a consequence, the packet residence time decreased with increasing sound pressure level and excess air velocity.

Figure 8 shows the effects of excess air velocity and sound pressure level on the fraction of time particle packets were in contact with the tube surface. The results demonstrate that the fraction of packet contact time decreased with increasing excess air velocity and sound pressure level, and this is due to increasing bubble frequency.

Figures 9–11 compare the bubble behavior for two powders (Fly Ash BW and Talc) with excess air velocity at different sound pressure levels. While both powders behave in a qualitatively similar fashion, the actual values of bubble frequency, packet residence time, and the fraction of packet contact time at given $U_o - U_{mb}$ and SPL_o depend strongly on material properties. Note that these powders have different size distributions, mean diameters, densities, particle shapes, and chemical compositions.

Gas film thickness at tube wall

Figure 12 shows the variation of gas film thickness with excess air velocity at $\theta = 90°$ for fly ash HC. The data show the gas film thickness increased slightly with excess air velocity and decreased slightly with an increase in sound pressure level.

Measurements with Talc and fly ash BW exhibited similar behavior, with l_g ranging from 45 μm to 90 μm depending on the material.

Heat transfer in a bubbling bed

To provide a benchmark for the heat-transfer measurements, the heated tube was tested in a fluidized bed of 820 μm glass beads with superficial air velocities ranging up to 110 cm/s. Figure 13 shows the comparison between the heat-transfer measurements and results from previous studies for glass beads. The data show that, beyond a superficial air velocity of 0.8 m/s, the average heat-transfer coefficient was independent of air velocity, and this result agrees with those from previous studies (Biyikli and Chen, 1982; Biyikli et al., 1982).

The 820 μm glass beads are Geldart B particles, and, because of their size, the authors did not expect to see any effect of sound on their behavior. This is verified by Figure 14, which shows a comparison of average heat-transfer coefficient with and without sound for these particles. The fluidizing behavior

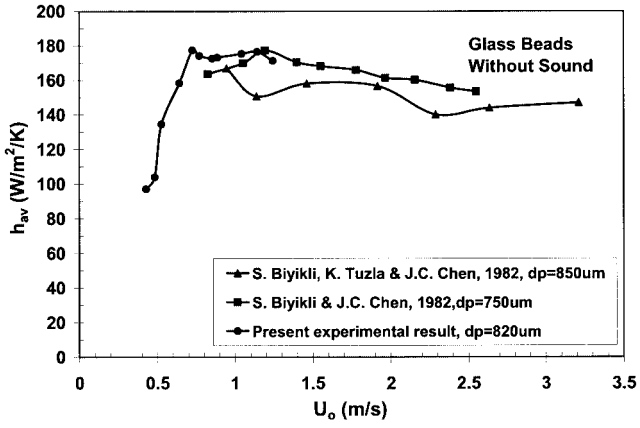

Figure 13. Comparison of average heat-transfer coefficients.

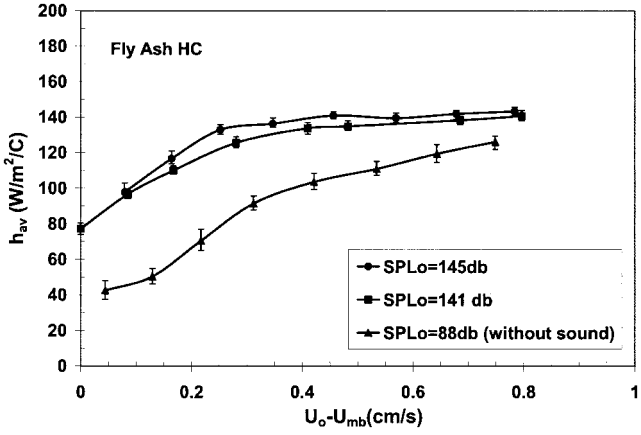

Figure 15. Variation of average heat-transfer coefficients with excess air velocity for fly ash HC.

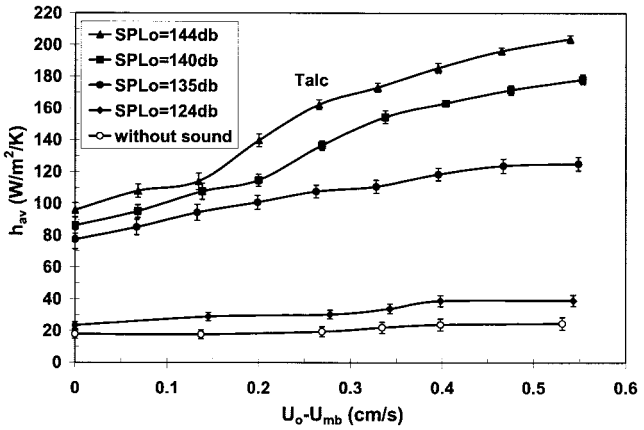

Figure 16. Variation of average heat-transfer coefficients with excess air velocity for talc.

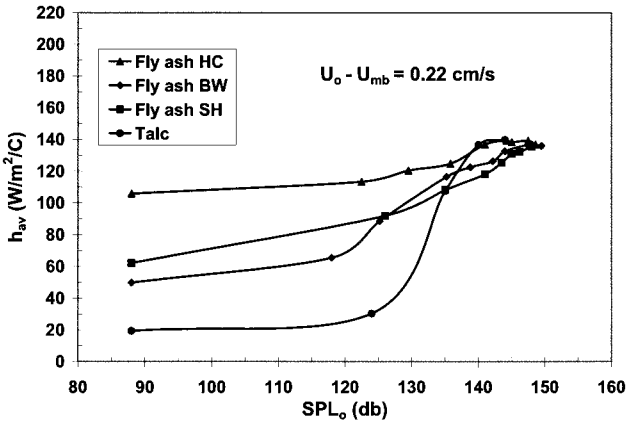

Figure 18. Variation of average heat-transfer coefficient with sound pressure level.

of large particles is not affected by an acoustic field, and, as a consequence, there is also no effect on heat transfer. As already noted, all the experiments were performed at a frequency of 80 Hz. Additional experiments would be needed to determine if the larger glass particles would respond to acoustic excitation of other frequencies.

Figure 15 shows the variation of average heat-transfer coefficient with excess air velocity for different sound pressure levels for fly ash HC, a type A powder. The data show that the average heat-transfer coefficient increased with increases in both excess air velocity and sound pressure level. The phenomena of more bubbles and greater agitation of the bed material were observed as the excess air velocity and sound pressure level increased.

Figure 16 shows the variation of average heat-transfer coefficients with excess air velocity for different sound pressure levels for Talc. The results were qualitatively the same as for fly ash HC. However, the Talc exhibited poor fluidization behavior at SPL_o = 124 db, and the average heat-transfer coefficient was relatively low. Nevertheless, once SPL_o increased to 135 db, the average heat-transfer coefficient was obviously improved.

Figure 17 summarizes the effect of sound pressure level and excess air velocity on the four types of A and C powders tested.

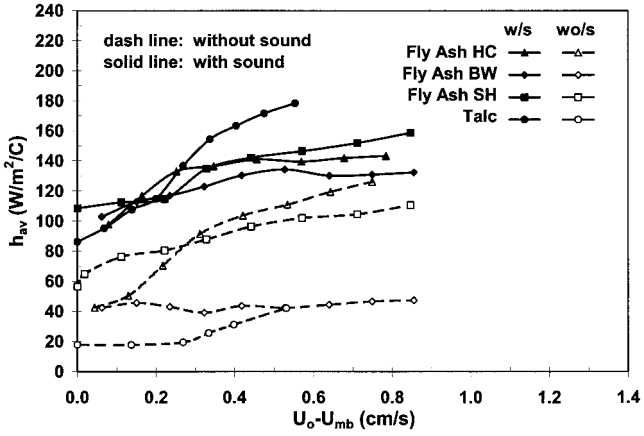

Figure 17. Variation of average heat-transfer coefficients with excess air velocity.

For experiments with sound, 144 < SPL_o < 145 db.

In all cases, the average heat-transfer coefficients were improved with sound assistance. In addition, with sound assistance, the average heat-transfer coefficients increased with an increase in excess air velocity. Without sound assistance, fly ash BW and Talc could not be fluidized, and as a consequence had significantly lower average heat-transfer coefficients. Fly ashes HC and SH could be fluidized both with and without sound, although the sound improved the average heat transfer coefficient for both materials.

Figure 18 shows the variation of average heat-transfer coefficient with sound pressure level with $U_o - U_{mb}$ held constant at 0.22 cm/s. The data demonstrate that, at a fixed excess air velocity, most of the increase in the average heat-transfer coefficient occurred between 125 and 140 db.

The orientation of a horizontal tube is shown in Figure 19. The angle indicates a counterclockwise location measured from the bottom of the tube. The local heat-transfer coefficients were determined at four positions around the tube perimeter (θ = 0°, 90°, 180°, and 270°). Figure 20 shows the variation of local heat-transfer coefficient with excess air velocity at fixed sound pressure levels for Talc. The lowest local heat-transfer coefficients were obtained at the top of the tube (θ = 180°), due to the stagnant particle layer which was present at that location. In addition, the data indicated that as excess air velocity increased, the values of heat-transfer coefficients at 0°, 90°, and 270° all approached the same value. In all cases for fly ash BW, fly ash SH, and fly ash HC, the same trends were obtained.

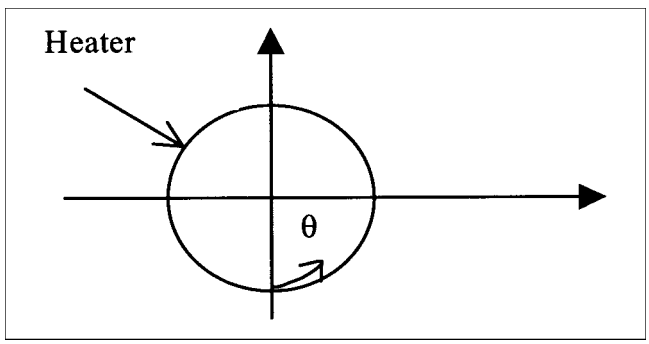

Figure 19. Orientation of the angle.

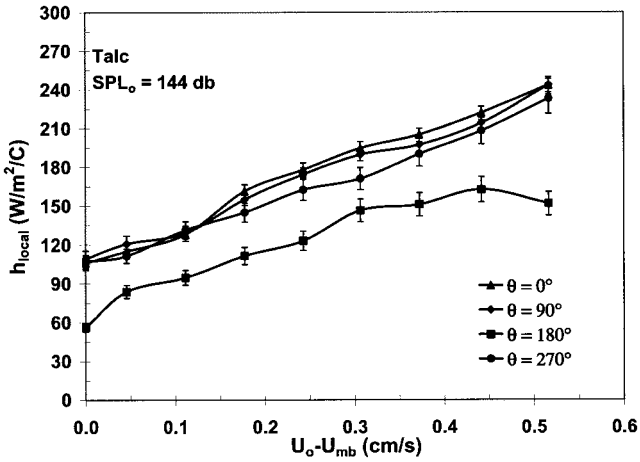

Figure 20. Variation of local heat-transfer coefficients with excess air velocity for talc.

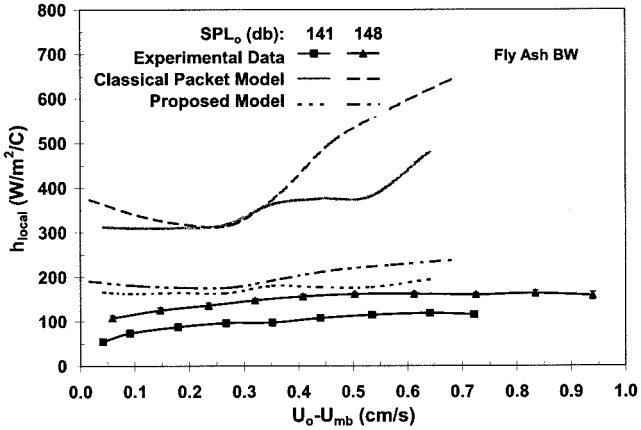

Figure 22. Comparison of local heat-transfer coefficients for packet renewal and proposed model.

Heat-transfer model comparison

For a period of particle contact with the tube, the time-average heat-transfer coefficient can be calculated by Eqs. 12 or 11 for the classical packet renewal or proposed models. During the period of time for the test, the particle packet periodically contacted with the heated surface. The overall time-average heat-transfer coefficient is evaluated by Eq. 17

$$\bar{h} \cdot \sum_{i=1}^{n} t_i = \sum_{i=1}^{n} \bar{h}_i \cdot t_i \qquad (17)$$

where t_i is each period of packet contact time at the surface, and $\bar{h}_i$ is the time-average heat-transfer coefficient for each contact at the surface.

Figures 21–23 show the comparison of the heat-transfer coefficients with the classical packet renewal model, the proposed model, and the experimental data for fly ash HC, fly ash BW, and Talc. From these figures, it is obvious that the classical packet renewal model gives a very poor prediction for the heat-transfer coefficient, while the proposed model gives much better agreement with the experimental data. The results confirm that the presence of a gas film between the heated surface and emulsion phase has a strong influence on heat-transfer coefficient.

Conclusions

Heat transfer and bubble behavior in a sound-assisted fluidized bed with a horizontal tube are described. From the experimental results, information on bubble behavior was obtained. The data show that bubble frequency increased with an increase in excess air velocity and a sound pressure level, and the packet residence time and the fraction of the packet contact time at the tube surface decreased with increasing excess air velocity and sound pressure level.

It was also found that a gas film is present in the vicinity of the tube surface. The gas film thickness increased slightly with increasing excess air velocity and decreased with an increase in sound pressure level. The convective heat-transfer coefficient between the tube surface and the bed material is strongly affected by the existence of the gas film between the heated surface and the emulsion phase.

The heat-transfer data showed that, for Geldart type B particles, the acoustic field does not affect heat-transfer coefficient. For Geldart A and C particles, the average heat-transfer coefficient increased with increasing excess air velocity. In

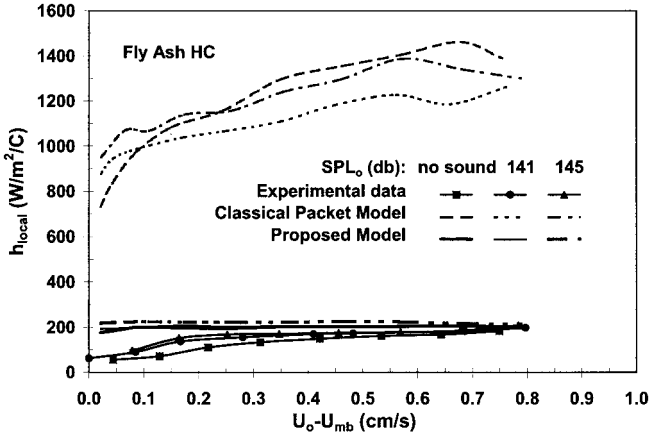

Figure 21. Comparison of local heat-transfer coefficients for packet renewal and proposed models.

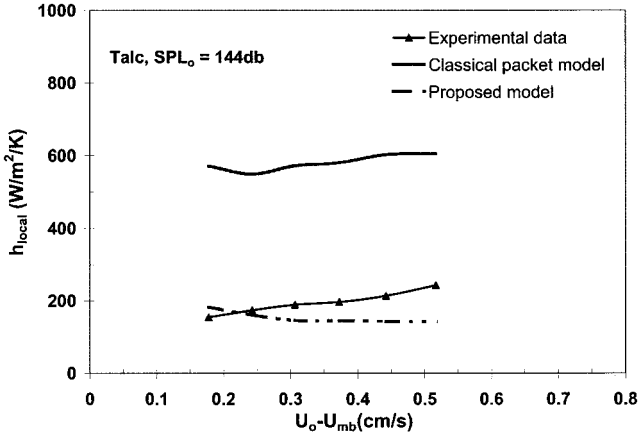

Figure 23. Comparison of local heat-transfer coefficients for packet renewal and proposed models.

addition, a higher sound pressure level contributes to an increase in the average heat-transfer coefficient.

Based on the existence of a gas film between the heated surface and emulsion phase, a packet renewal model with a gas film at the tube surface was proposed to explain the heat-transfer data, and a modified heat-transfer coefficient equation was developed. The proposed model results in heat-transfer coefficient predictions, which are much closer to the experimental data than those obtained from the classical packet renewal model.

Notation

A = constant in heat-transfer coefficient Eq. 9, $\frac{1}{2}\sqrt{\pi\rho_d c_d k_d}$
A_s = surface area of the heater, m^2
c_p = specific heat of solid particle, J/kg/K
$\overline{d_p}$ = mean particle diameter, μm
d_i = arithmetical particle diameter between the $(i-1)$ and i, μm
F_b = fraction of total time for bubble phase at the surface
F_d = fraction of total time for emulsion phase (or dense phase) at the surface, which is equal to $(1-F_b)$
h = heat transfer coefficient in the fluidized bed, W/m^2/K
h_{av} = average heat-transfer coefficient, W/m^2/K
h_d = convective heat-transfer coefficient for emulsion (dense) phase, W/m^2/K
$\overline{h_d}$ = time-average heat-transfer coefficient for emulsion (dense) phase, W/m^2/K
h_{local} = local heat-transfer coefficient, W/m^2/K
k_d = thermal conductivity of the emulsion phase, W/m/K
k_g = thermal conductivity of gas, W/m/K
k_p = thermal conductivity of solid particle, W/m/K
l_g = gas film thickness, mm
Q = heat generation, W
q''_o = heat flux, W/m^2
R = electrical resistance, ohm
SPL_o = sound pressure level at the distributor plate, db
t_p = packet residence time, s
T_B = bed temperature, K
T_g = gas temperature, K
T_s = surface temperature of heater, K
T_W = wall temperature, K
U_{mb} = minimum bubbling velocity, cm/s
U_o = superficial air velocity, cm/s
V = root-mean-square voltage, volt
x_i = the fraction of weight for the i-th particle size
α_d = thermal diffusivity of the emulsion (dense) phase, $k_d/\rho_d c_d$, m^2/s
ρ_d = density of the emulsion phase, kg/m^3
ρ_p = particle density, kg/m^3
θ = angular position around the tube, measured counterclockwise from the bottom of the tube

Literature Cited

Adams, R. L., and J. R. Welty, "A Gas Convection Model of Heat Transfer in Large Particle Fluidized Beds," *AIChE J.,* **25**(3), 395 (1979).

Biyikli, S., and J. C. Chen, "Effect of Mixed Particle Sizes on Local Heat Transfer Coefficients around a Horizontal Tube in Fluidized Beds," 7th Int. Heat Transfer Conf., Munich (Sept. 6–10, 1982).

Biyikli, S., K. Tuzla, and J. C. Chen, "Heat Transfer Around a Horizontal Tube in Freeboard Region of Fluidized Beds," Paper No. 826, AIChE Meeting, Los Angeles (Nov. 14–19, 1982).

Botterill, J. S. M., *Fluid-Bed Heat Transfer,* Academic Press, New York (1975).

Chandran, R., J. C. Chen, and F. W. Staub, "Local Heat Transfer Coefficients Around Horizontal Tubes in Fluidized Bed," *J. Heat Transfer,* **102,** 152 (1980).

Chen, J. C., "Heat Transfer to Submersed Tubes in Fluidized Beds," *Two-Phase Flow and Heat Transfer,* China-U.S. Progress, Hemisphere Publishing Corporation, New York, p. 505 (1984).

Chen, J. C., and K. Tuzla, "Heat Transfer to Immersed Surfaces in Bubbling Fluidized Beds," *Ann. Rev. of Heat Transfer,* **7,** 407 (1996).

Chirone, R., and L. Massimilla, "Sound-Assisted Aeration of Beds of Cohesive Solids," *Chem. Eng. Sci.,* **49**(8), 1185 (1994).

Decker, N., and L. R. Glicksman, "Heat Transfer in Large Particle Fluidized Bed," *Int. J. Heat Mass Transfer,* **26**(9), 1307 (1983).

Grewal, N. S., and S. C. Saxena, "Heat Transfer Between a Horizontal Tube and a Gas-Solid Fluidized Bed," *Int. J. Heat Mass Transfer,* **23,** 1505 (1980).

Herrera, C., "Acoustic Characteristics of Fine Powders in Fluidized Beds," PhD Diss. Lehigh University (2000).

Herrera, C., E. Levy, and J. Ochs, "Characteristics of Acoustic Standing Waves in Fluidized Beds," *AIChE J.,* **48**(3), 503 (2002).

Incropera, F. P., and D. P. DeWitt, *Fundamentals of Heat and Mass Transfer,* 4th ed., Wiley, New York (1999).

Kunii, D., and J. M. Smith, "Heat Transfer Characteristics of Porous Rocks," *AIChE J.,* **6**(1), 71 (1960).

Mickley, H. S., and D. F. Fairbanks, "Mechanism of Heat Transfer to Fluidized Bed," *AIChE J.,* **1**(3), 374 (1955).

Miyamoto, M., R. Jin, Y. Katoh, and J. Kurima, "Heat Transfer Characteristics and Particle Behavior Around Circular Tubes Immersed in Fluidized Beds," *Heat Transf.—Japanese Res.,* **26**(5), 306 (1997).

Morse, R. D., "Sonic Energy in Granular Solid Fluidization," *Ind. Eng. Chem.,* **47,** 1170 (1955).

Moslemian, D., M. M. Chen, and B. T. Chao, "Heat Transfer to Horizontal Tubes in a Fluidized Bed: The Role of Superficial Gas and Local Particle Velocities," *Experimental Thermal and Fluid Science,* **4,** 76 (1991).

Olsson, S. E., and A. E. Almstedt, "Local Instantaneous and Time-Average Heat Transfer in a Pressured Fluidized Bed with Horizontal Tube: Influence of Pressure, Fluidization Velocity and Tube-Bank," *Chem. Eng. Sci.,* **50**(22), 3231 (1995).

Ozkaynak, T. F., and J. C. Chen, "Emulsion Phase Residence Time and Its Use in Heat Transfer Models in Fluidized Beds," *AIChE J.,* **26**(4), 544 (1980).

Ranz, W. E., "Friction and Transfer Coefficients for Single Particles and Packed Beds," *Chem. Eng. Prog.,* **48**(5), 247 (1954).

Russo, P., R. Chirone, L. Massimilla, and S. Russo, "The Influence of the Frequency of Acoustic Waves on Sound-Assisted Fluidization of Beds of Fine Particles," *Powder Technol.,* **82,** 219 (1995).

Vreedenberg, H. A., "Heat Transfer Between a Fluidized Bed and a Horizontal Tube," *Chem. Eng. Sci.,* **9**(1), 52 (1958).

Wen, C. Y., and Y. H. Yu, "A Generalized Method for Predicting the Minimum Fluidization Velocity," *AIChE J.,* **12**(3), 610 (1966).

Wiman, J., and A. E. Almstedt, "Hydrodynamics, Erosion and Heat Transfer in a Pressured Fluidized Bed: Influence of Pressure, Fluidization Velocity, Particle Size and Tube Bank Geometry," *Chem. Eng. Sci.,* **52**(16), 2677 (1997).

Appendix

Effective (root mean square) pressure

The effective pressure p_e, is the overall measurement of the amplitude of the sound pressure, defined by

$$p_e = \frac{|p(x,\,t)|}{\sqrt{2}} = \frac{P}{\sqrt{2}}$$

where P is the absolute magnitude of the sound pressure $P = |p(x,\,t)|$.

Sound pressure level

The sound pressure level describes the sound quantity through the use of a logarithmic scale, defined by

$$\text{SPL} = 20 \cdot \log\left[\frac{p_e}{p_{\text{ref}}}\right]$$

where p_{ref}, the reference pressure, is the value of the threshold of human hearing, which is $p_{\text{ref}} = 2 \times 10^{-5}$ Pa.

Manuscript received Dec. 6, 2002, revision received June 11, 2003, and final revision received Sept. 29, 2003.